Letters

High-Efficiency, High-Power Asymmetrically Designed Three-Phase Power Supply for Electrolytic Hydrogen Production

Hanlei Tian, *Graduate Student Member, IEEE*, Wei Han, *Member, IEEE*, Jagabar Sathik M, *Senior Member, IEEE*, Maolin Chen, *Graduate Student Member, IEEE*, Guozhuang Liang, *Member, IEEE*, and Saad Mekhilef, *Fellow, IEEE*

***Abstract*—This article presents a parallel 24-pulse rectifier employing dual non-phase-shifted transformers (DNPST) to efficiently address the cost-effectiveness and high-power requirements in the electrolytic hydrogen production, with the characteristics of low-voltage and high-current demands. The proposed method injects voltage harmonics, generated by harmonic injection circuits, into the dc side of the rectifier through two specially designed asymmetric DNPST. It brings an almost sinusoidal input current and an output current with 2.5% ripple rate of the rectifier, significantly improving the power quality. Furthermore, the two small-capacity injection circuits are capable of performing phase shifting, thus eliminating the need for phase-shifting transformers. Finally, both simulated and experimental results are given to validate the effectiveness of the proposed system.**

***Index Terms*—Current ripple, electrolysis hydrogen production, green energy, multipulse rectifier.**

Received 13 July 2024; revised 31 August 2024; accepted 16 September 2024. Date of publication 19 September 2024; date of current version 12 December 2024. This work was supported in part by Guangzhou Science and Technology Plan Project under Grant 2023A04J0311 and in part by Guangzhou-HKUST(GZ) Joint Funding Program under Grant 2024A03J0680. *(Corresponding author: Wei Han.)*

Hanlei Tian is with the Sustainable Energy and Environment Thrust, The Hong Kong University of Science and Technology, Guangzhou 511453, China (e-mail: thledu@ieee.org).

Wei Han is with the Sustainable Energy and Environment Thrust, The Hong Kong University of Science and Technology, Guangzhou 511453, China, and also with the Department of Electronic and Computer Engineering, The Hong Kong University of Science and Technology, Hong Kong (e-mail: weihan@kust-gz.edu.cn).

Jagabar Sathik M is with the Faculty of Engineering and Technology, SRM Institute of Science and Technology,, Tamil Nadu 603203, India (e-mail: mjsathik@ieee.org).

Maolin Chen is with the College of Electrical Engineering, Sichuan University, Chengdu 610065, China (e-mail: chenml@alu.scu.edu.cn).

Guozhuang Liang is with the School of Electrical Engineering, Hebei University of Science and Technology, Shijiazhuang 050091, China (e-mail: guozhuangliang@hebust.edu.cn).

Saad Mekhilef is with the Power Electronics and Renewable Energy Research Laboratory, Department of Electrical Engineering, University of Malaya, Kuala Lumpur 50603, Malaysia, also with the School of Science, Computing and Engineering Technologies, Swinburne University of Technology, Hawthorn, VIC 3122, Australia, and also with the Department of Electrical and Electronics Engineering, Presidency University, Bengaluru, Karnataka 560064, India (e-mail: smekhilef@swin.edu.au).

Color versions of one or more figures in this article are available at https://doi.org/10.1109/TPEL.2024.3464675.

Digital Object Identifier 10.1109/TPEL.2024.3464675

I. Introduction

HYDROGEN, as a clean and efficient energy carrier, holds significant potential for reducing greenhouse gas emissions, promoting sustainable development, and enhancing energy security [1], [2]. Compared with traditional methods, electrolytic hydrogen production has garnered widespread attention due to its environmental friendliness, diverse energy sources, high-purity hydrogen production, and rapid response characteristics [3]. However, the high energy consumption associated with large-scale hydrogen production and the additional losses caused by dc ripple in the electrolytic cell (EC) have made hydrogen production efficiency a critical concern.

Various power converters have been adapted for use in ECs, falling into the categories of high-frequency, medium-frequency, and line-frequency methods. In the high-frequency approach, effective control of both dc-side current ripple and ac-side current harmonics enhances the hydrogen production efficiency of ECs [4]. However, the cost of this method is notably higher compared with diode or thyristor rectifiers with equivalent power ratings. To reduce active switch count, a medium-frequency converter operating at 600 Hz has been suggested. Nevertheless, with a total harmonic distortion (THD) of the input current reaching up to 17%, it fails to meet harmonic standards, such as IEEE-519 and IEC-61000-3-2. In the realm of line-frequency methods, 12-pulse rectifiers are widely employed in high-power applications requiring high reliability due to their simple structure, robust overload capacity, and low electromagnetic interference [5]. However, the THD of up to 15.2% poses a barrier to their direct integration into microgrids. Presently, two primary solutions are being explored to tackle this challenge. The first involves augmenting the number of phase-shifting transformers and altering the winding method to increase the number of pulses [6]. Nevertheless, due to the intricate structure and elevated manufacturing costs of phase-shifting transformers, widespread implementation of this solution remains a formidable task.

In light of this, an alternative solution employs dc-side passive current modulation technology. This technology utilizes an advanced tap reactor to generate a square-wave circulating current on the dc side, effectively counteracting low-order harmonics in the input current [7]. Consequently, it doubles the rectifier pulse number, suppresses grid-side harmonics, and reduces the output

current ripple. In [8], the passive current injection circuit based on dual auxiliary transformers is proposed, generating a specific square-wave current that modulates the input current from 12 pulses to 24 pulses. Two large capacitors are required on the dc side of the rectifier to provide a neutral point. These capacitors endure high current stress, increasing losses, and reducing the rectifier's lifetime. In this regard, a novel 24-pulse rectifier is proposed by combining a conventional tap converter (CTC) and an improved tap converter [9], [10], [11]. This method is simple in structure and easy to implement. However, the harmonic suppression capability of the CTC is limited, and its auxiliary diodes, connected in series in the load path, endure high current due to the hydrogen production yield being directly proportional to the mean value of the dc current. Furthermore, an auxiliary single-phase full-wave rectifier is proposed and installed in parallel on the dc side [12]. Consequently, the current flowing through the auxiliary diode constitutes only 3.4% of the load current. However, this configuration necessitates that the two double-star transformers provide a 30° phase shift at the secondary side.

In response to the aforementioned issues, this letter proposes a parallel 24-pulse rectifier based on dual non-phase-shifted transformers (DNPSTs) to achieve high-power, low-cost, and efficient electrolytic hydrogen production. The designed asymmetric harmonic injection circuits not only enable the operation of the DNPST but also upgrade the system from 12 pulses to 24 pulses. As a result, the current harmonic decreases to 5.2%, and the ripple decreases to 2.5%. Compared with the voltage injection method in [11], the proposed passive pulse multiplication circuit (PPMC) is a pure current injection method, which eliminates the need for large inductors on the ac side. Furthermore, the overall parallel design enhances fault tolerance, making it more suitable for high-current hydrogen production scenarios.

II. Topology of Proposed System for Hydrogen Production

A. Topology Analysis of Proposed Rectifier

The proposed topology consists of a three-phase ac source, two six-pulse rectifiers, two passive pulse multiplication circuits (PPMC1 and PPMC2), and a balanced reactor, as shown in Fig. 1(a). PPMC1 and PPMC2 are composed of an injection transformer and two auxiliary diodes, respectively. Fig. 1(b) shows the winding structures of the transformers T_1 and T_2, using the delta-wye-wye connection. From Fig. 1(b), T_1 and T_2 have the same winding structure and do not require a phase-shifting design, thanks to the asymmetric design of PPMC1 and PPMC2.

The auxiliary diode of PPMC1 alternates conduction based on the relationship between the injected transformer's secondary-side voltage and the load voltage. A specific square-wave current is generated and injects it into the outputs of the rectifier. This configuration doubles the original 6-pulse output to 12 pulses. Similarly, PPMC2 doubles the original 6-pulse output to 12 pulses. Meanwhile, due to the asymmetric structure of PPMC1 and PPMC2, two sets of 12 pulses are connected in parallel with a balanced reactor, achieving a 24-pulse output, as shown in Fig. 2.

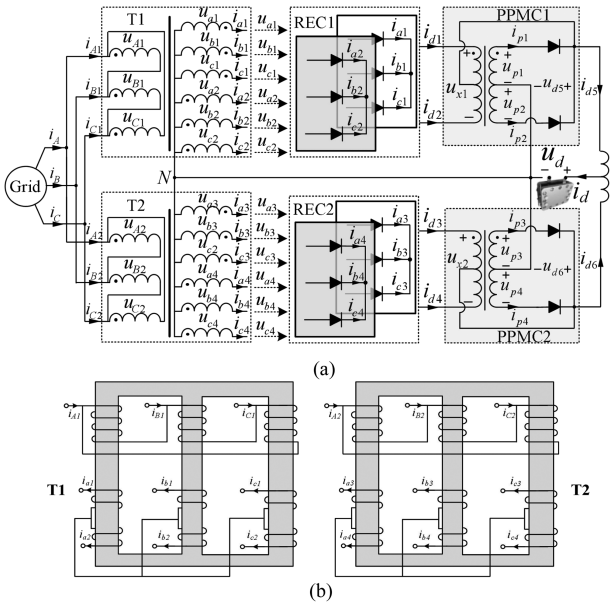

Fig. 1. Topology display. (a) Main circuit of the proposed hydrogen production rectifier. (b) Winding structures of T_1 and T_2.

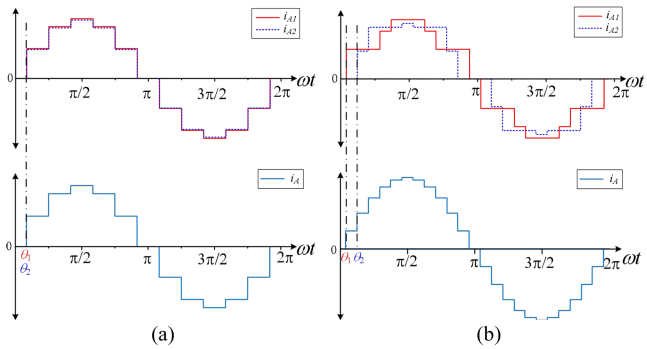

Fig. 2. Principle of pulse-wave multiplication. (a) Symmetrical structure. (b) Proposed asymmetric structure.

First, the turn ratio of PPMC1 to PPMC2 is defined as follows:

$$m_1 = \frac{u_{p1}}{u_{x1}}, \quad m_2 = \frac{u_{p3}}{u_{x2}} \tag{1}$$

where u_{p1}, u_{p3}, u_{x1}, and u_{x2} represent the secondary winding voltage and primary winding voltage of PPMC1 and PPMC2, respectively.

B. Mode Analysis of PPMC

Due to the function of the balanced reactor, both PPMC1 and PPMC2 can operate independently and are decoupled from each other. As a result of space constraints, this section focuses solely on examining the operational mode of PPMC1. By exploring the interplay among the injected voltage, load voltage, and rectifier current, PPMC1 can be categorized into three distinct operational modes, as illustrated in Fig. 3.

Mode I: When $-u_{p1} > u_{d5}$, PPMC1 operates in Mode I. The auxiliary diode D_1 is reverse biased, and the auxiliary diode D_2 conducts. At this time, the circuit operates, as illustrated in Fig. 3(a). According to Kirchhoff's voltage law (KVL) and

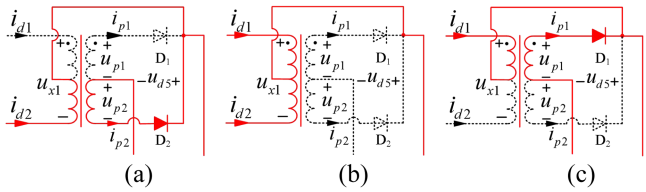

Fig. 3. Working modes of PPMC1. (a) Mode I. (b) Mode II. (c) Mode III.

Kirchhoff's current law (KCL), the input current and output voltage of PPMC1 satisfy

$$\begin{cases} i_{d1}=0 \\ i_{d2}=\frac{2m_1}{2m_1+1}I_{d5} \end{cases} \begin{cases} i_{p1}=0 \\ i_{p2}=\frac{1}{2m_1+1}I_{d5} \end{cases} \begin{cases} u_{d5}=\frac{2m_1}{2m_1+1}u_{d2} \\ u_{d1}=\frac{2m_1-1}{2m_1+1}u_{d2}. \end{cases} \tag{2}$$

Mode II: When $|u_{p1}|<u_{d5}$, PPMC1 operates in Mode II. The auxiliary diodes are all reverse biased. At this time, the working mode of the circuit is shown in Fig. 3(b). According to KVL and KCL, the input current and output voltage of PPMC1 satisfy

$$i_{d1}=i_{d2}=\frac{I_{d1}}{2}, i_{p1}=i_{p2}=0, u_{d5}=\frac{u_{d1}+u_{d2}}{2}. \tag{3}$$

Mode III: When $u_{p1}>u_{d5}$, PPMC1 operates in Mode III. The auxiliary diode D_2 is reverse biased, and the auxiliary diode D_1 conducts, as shown in Fig. 3(c). Similarly, the input current and output voltage of PPMC1 satisfy

$$\begin{cases} i_{d1}=\frac{2m_1}{2m_1+1}I_{d5} \\ i_{d2}=0 \end{cases} \begin{cases} i_{p1}=\frac{1}{2m_1+1}I_{d5} \\ i_{p2}=0 \end{cases} \begin{cases} u_{d5}=\frac{2m_1}{2m_1+1}u_{d1} \\ u_{d2}=\frac{2m_1-1}{2m_1+1}u_{d1} \end{cases} \tag{4}$$

where u_{d1}, u_{d2}, and I_{d5} represent the output voltage of rectifier bridge REC1 and the output current of PPMC1, respectively. Also, the relationship with the output voltage meets

$$I_{d5}=I_{d6}=\frac{I_d}{2}. \tag{5}$$

III. Performance Analysis

A. THD Analysis of Hydrogen Production Power Supply

Based on the analysis of the operating modes and the structure of the proposed rectifier, as shown in Fig. 1, the grid-side current i_A can be calculated as

$$i_A=\begin{cases} 0, & \omega t\in[0,\theta_1) \\ \frac{kI_d}{4}, & \omega t\in[\theta_1,\theta_2) \\ \frac{kI_d}{2}, & \omega t\in[\theta_2,\frac{\pi}{3}-\theta_2) \\ \frac{kI_d}{4}+\frac{km_2I_d}{2m_2+1}, & \omega t\in[\frac{\pi}{3}-\theta_2,\frac{\pi}{3}-\theta_1) \\ \frac{km_2I_d}{2m_2+1}+\frac{km_1I_d}{2m_1+1}, & \omega t\in[\frac{\pi}{3}-\theta_1,\frac{\pi}{3}+\theta_1) \\ \frac{km_2I_d}{2m_2+1}+\frac{kI_d}{2} & \omega t\in[\frac{\pi}{3}+\theta_1,\frac{\pi}{3}+\theta_2) \\ kI_d & \omega t\in\left[\frac{\pi}{3}+\theta_2,\frac{\pi}{2}\right]. \end{cases} \tag{6}$$

According to (6), Fig. 4 illustrates the relationship curve between the injected transformer turn ratio and the grid-side current harmonics, obtained through MATLAB. When the turn ratios satisfy $m_1=2.07$ and $m_2=6.33$, the grid-side harmonic current is minimized to 7.58%.

Considering the asymmetric design of PPMC1 and PPMC2, there is a deviation in the voltage rms at both ends of the balanced

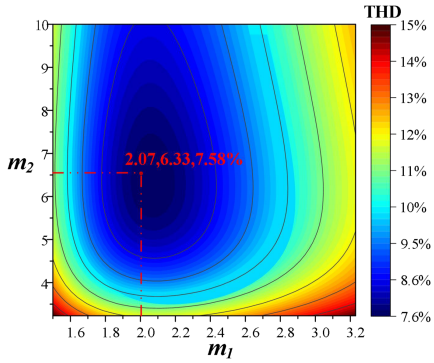

Fig. 4. Relationship between THD and turn ratio.

reactor, which may lead to the issue of dc magnetization. To address this, the transformers T_1 and T_2 have been redesigned to ensure that the voltage rms is equal. Specifically, according to the mode analysis, the relationship between the output voltages and their turn ratios m_1 and m_2 can be calculated as follows:

$$u_{d5,d6}=\begin{cases} \frac{2m_{1,2}}{2m_{1,2}+1}k_{1,2}U_m\sin(\omega t+\frac{\pi}{2}) & \omega t\in[0,\theta_{1,2}] \\ \frac{3}{2}k_{1,2}U_m\sin(x+\frac{\pi}{3}) & \omega t\in[\theta_{1,2},\frac{\pi}{3}-\theta_{1,2}] \\ \frac{2m_{1,2}}{2m_{1,2}+1}k_{1,2}U_m\sin(\omega t+\frac{\pi}{6}) & \omega t\in[\frac{\pi}{3}-\theta_{1,2},\frac{\pi}{3}+\theta_{1,2}] \\ \frac{3}{2}k_{1,2}U_m\sin(x) & \omega t\in[\frac{\pi}{3}+\theta_{1,2},\frac{2\pi}{3}-\theta_{1,2}] \\ \frac{2m_{1,2}}{2m_{1,2}+1}k_{1,2}U_m\sin(\omega t-\frac{\pi}{6}) & \omega t\in[\frac{2\pi}{3}-\theta_{1,2},\frac{2\pi}{3}] \end{cases} \tag{7}$$

where U_m is the rms of the grid-side line voltage. k_1 and k_2 are the turn ratios of transformers T_1 and T_2, respectively.

According to (6) and (7), when the rms of the output voltage of PPMC1 and PPMC2 is equal, the ratios of transformers T_1 and T_2 should meet the following requirements:

$$\frac{k_2}{k_1}=0.933. \tag{8}$$

B. Capacity Analysis of PPMC

According to the mode analysis, the input voltages of PPMC1 and PPMC2 can be calculated as follows:

$$u_{x1,x2}=\begin{cases} \frac{-2\sqrt{3}}{2m_{1,2}+1}k_{12}U_m\sin(\omega t+\frac{\pi}{2}) & \omega t\in[0,\theta_{1,2}] \\ -\sqrt{3}k_{12}U_m\cos(x+\frac{\pi}{3}) & \omega t\in[\theta_{1,2},\frac{\pi}{3}-\theta_{1,2}] \\ \frac{2\sqrt{3}}{2m_{1,2}+1}k_{12}U_m\sin(\omega t+\frac{\pi}{6}) & \omega t\in[\frac{\pi}{3}-\theta_{1,2},\frac{\pi}{3}+\theta_{1,2}] \\ \sqrt{3}k_{12}U_m\cos(\omega t) & \omega t\in[\frac{\pi}{3}+\theta_{1,2},\frac{2\pi}{3}-\theta_{1,2}] \\ \frac{-2\sqrt{3}}{2m_{1,2}+1}k_{12}U_m\sin(\omega t-\frac{\pi}{6}) & \omega t\in[\frac{2\pi}{3}-\theta_{1,2},\frac{2\pi}{3}]. \end{cases} \tag{9}$$

Substituting the optimal turn ratio into (9), the rms of PPMC1 and PPMC2 is given as follows:

$$U_{x1\_\mathrm{rms}}=0.328U_d, \qquad U_{x2\_\mathrm{rms}}=0.145U_d. \tag{10}$$

TABLE I
COMPARISON RESULTS BETWEEN THE PROPOSED METHOD AND SIMILAR WORKS

Indicators		Conventional 24-pulse method	Proposed in [9]	Proposed in [10]	Proposed in [11]	Proposed in [12]	Proposed in [13]	Proposed method
THD of input current		≈5%	7.57%	7.57%	3.03%	7.57%	3.0%	5.2%
AC and DC side is isolated or not		Yes	Yes	Yes	No	Yes	Yes	Yes
Efficiency of rectifier		≈97%	98.2%	96.2%	96.6%	96.4%	95.6%	98.2%
Power density		-	-	4.2 W/in^3	7.18 W/in^3	3.5 W/in^3	4.92 W/in^3	4.6 W/in^3
Stability of output voltage		Good	Good	Good	Bad	Good	Bad	Good
Harmonic suppression method		/	Current injection	Current injection	Voltage injection	Current injection	Voltage injection	Current injection
Number of components	Number of output side capacitors	0	0	0	2	0	2	0
	Number of output side diodes	24 (main)	12 (main) 2 (series) 2 (parallel)	12 (main) 8 (series)	12 (main) 4 (parallel)	12 (main) 2 (series)	12 (main) 2 (parallel)	12 (main) 4 (parallel)
Phase-shifting transformer	Phase-shifting design is necessary	Yes	Yes	Yes	Yes	Yes	Yes	No
	Connection type	Delta-wye-wye or Star-delta etc	Delta-wye-wye	Delta-wye-wye	Star-delta	Delta-wye-wye and 3*wye	Delta-delta-wye	Delta-wye-wye
Overall magnetic ratings		>210%	134%	145.9%	48.2%	180%	125.0%	129.7%
Application scenarios		Low, medium ,and high voltage, high power	Medium and high voltage, high power	Medium and high voltage, high power	Low and Medium voltage, high power	Electrolysis , and other low voltage, high current	High voltage and constant current load	Electrolysis, and other low voltage, high current

Note: Ref. [10] for calculating voltage stability. / indicates that the method has not been adopted. - means that the parameter does not exist.

Similarly, the input currents of PPMC1 and PPMC2 are calculated as follows:

$$i_{d1,3}=\begin{cases}0 & \omega t\in[0,\theta_{1,2})\cup[\frac{2\pi}{3}-\theta_{1,2},\frac{2\pi}{3}]\\ \frac{I_d}{4} & \omega t\in[\theta_{1,2},\frac{\pi}{3}-\theta_{1,2})\cup[\frac{\pi}{3}+\theta_{1,2},\frac{2\pi}{3}-\theta_{1,2})\\ \frac{m_{1,2}I_d}{2m_{1,2}+1} & \omega t\in[\frac{\pi}{3}-\theta_{1,2},\frac{\pi}{3}+\theta_{1,2}).\end{cases} \tag{11}$$

From (11), the input current rms of PPMC1 and PPMC2 can be calculated as

$$I_{d1\_\mathrm{rms}}=I_{d2\_\mathrm{rms}}=0.259I_d,\qquad I_{d3\_\mathrm{rms}}=I_{d4\_\mathrm{rms}}=0.309I_d. \tag{12}$$

According to the working principle of PPMC, the secondary current of PPMC1 and PPMC2 can be calculated as

$$i_{p1,p3}=\begin{cases}0 & \omega t\in[0,\frac{\pi}{3}-\theta_{1,2}]\\ \frac{1}{4m_{1,2}+2}I_d & \omega t\in[\frac{\pi}{3}-\theta_{1,2},\frac{\pi}{3}+\theta_{1,2}]\\ 0 & \omega t\in[\frac{\pi}{3}+\theta_{1,2},\frac{2\pi}{3}].\end{cases} \tag{13}$$

Similarly, the rms of the output current for PPMC1 and PPMC2 is

$$I_{p1\_\mathrm{rms}}=I_{p2\_\mathrm{rms}}=0.034I_d,\qquad I_{p3\_\mathrm{rms}}=I_{p4\_\mathrm{rms}}=0.022I_d. \tag{14}$$

Hence, the capacity of PPMC1 and PPMC2 can be calculated as

$$S_{\mathrm{PPDC1}}=\frac{1}{2}\left[\frac{1}{2}U_{x1\_\mathrm{rms}}I_{d1\_\mathrm{rms}}+\frac{1}{2}U_{x1\_\mathrm{rms}}I_{d2\_\mathrm{rms}}+m_1U_{x1\_\mathrm{rms}}I_{p1\_\mathrm{rms}}+m_1U_{x1\_\mathrm{rms}}I_{p2\_\mathrm{rms}}\right]=6.6\% \tag{15}$$

$$S_{\mathrm{PPDC2}}=\frac{1}{2}\left[\frac{1}{2}U_{x2\_\mathrm{rms}}I_{d3\_\mathrm{rms}}+\frac{1}{2}U_{x2\_\mathrm{rms}}I_{d4\_\mathrm{rms}}+m_1U_{x2\_\mathrm{rms}}I_{p3\_\mathrm{rms}}+m_1U_{x2\_\mathrm{rms}}I_{p4\_\mathrm{rms}}\right]=4.3\%. \tag{16}$$

IV. COMPARATIVE ANALYSIS WITH SIMILAR 24-PULSE METHODS

To illustrate the strengths and weaknesses of the proposed method, Table I presents a comparison with similar works discussed in [8], [9], [10], [11], [12], and [13].

From the perspective of the cost, the total cost of the multipulse rectifier is primarily determined by the capacity of the magnetic devices, creating a direct proportional relationship between the total cost and the capacity of these devices. Compared with the conventional 24-pulse method, the asymmetric structures proposed in this article, as shown in Table I, replace the need for multiple phase-shifting transformers, significantly reducing the total magnetic ratings. Compared with [11], the proposed method has a higher total magnetic rating. However, the method in [11], which is based on voltage injection, requires three large inductors to be connected in series on the input side of the rectifier to achieve harmonic suppression. These inductors not only reduce the displacement factor of the rectifier but also soften its output characteristics.

From the perspective of stability, the use of large capacitors in [11] and [13] not only increases capacitor losses but also reduces the lifespan of the rectifier. Additionally, the auxiliary diodes are subjected to significant current stress, resulting in substantial conduction losses. In contrast, the proposed method in this article avoids using capacitors as components in the injection circuit, and its symmetrical topology and the analysis of PPMC in Fig. 4 both demonstrate the fault tolerance.

From the design complexity, the complexity of the rectifier structure is primarily determined by the phase-shifting transformer's complexity. In comparison with the methods described in [9], [10], [11], [12], and [13], the proposed method in this article utilizes an asymmetric design of the pulse multiplication circuit, thereby eliminating the need for a phase-shifting design in the transformer. As a result, the complexity of the design in this article has been reduced.

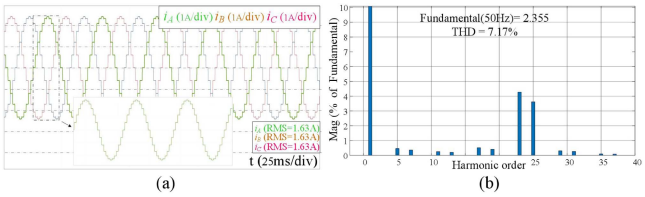

Fig. 5. Power quality analysis. (a) Simulation result of input current of the proposed scheme. (b) Harmonic order of the proposed method.

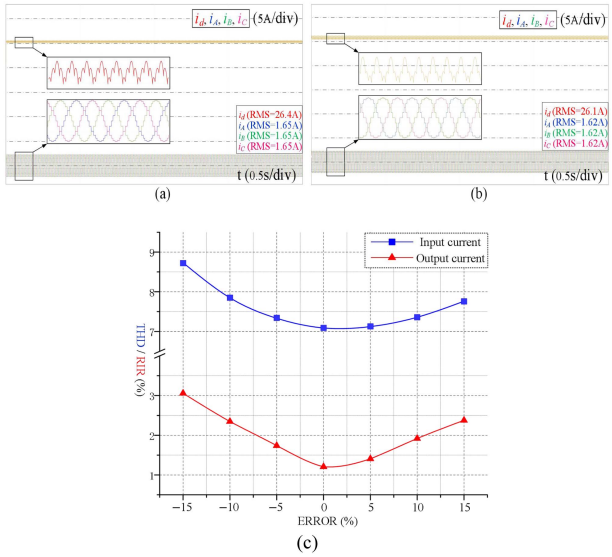

Fig. 6. Power performance analysis. (a) Considering fault tolerance of +10% in PPMC. (b) Considering fault tolerance of −10% in PPMC. (c) Power quality under different fault-tolerant conditions.

From the perspective of the application scenario, hydrogen production requires a low voltage and high current, as the hydrogen production rate is almost directly proportional to the current amplitude. Thus, high-current levels prevent semiconductor devices from being directly connected in series with the load. In comparison with the methods discussed in [9], [10], and [12], the parallel structure proposed in this article is more practical for such conditions due to its lower conduction losses and greater capacity to handle the high current.

V. Results and Discussion

A. Simulation Analysis

The proposed method is simulated using PSIM software. And, the parameters of theoretical analysis were adopted in this simulation. The results of input current under different conditions are measured. From Fig. 5(a), a clear 24-step input current is presented through the proposed hydrogen production power supply, and the THD, as shown in Fig. 5(b), is 7.17%.

For power performance analysis, the fault tolerance of the proposed rectifier is examined. Fig. 6(a) and (b) presents the input and output currents, respectively, accounting for the error margins of +10% and −10% in the PPMC configuration. The simulation results indicate that the ripples of the output current are 1.89% and 2.39%, respectively, and the harmonics of the input current are 7.39% and 7.83%, respectively. Practically, the THD is expected to reduce further due to the presence of leakage inductance in actual production. Furthermore, Fig. 6(c) presents the THD and the ripple rate under various levels of fault tolerance. As observed in Fig. 6(c), the proposed method consistently sustains a high level of power quality.

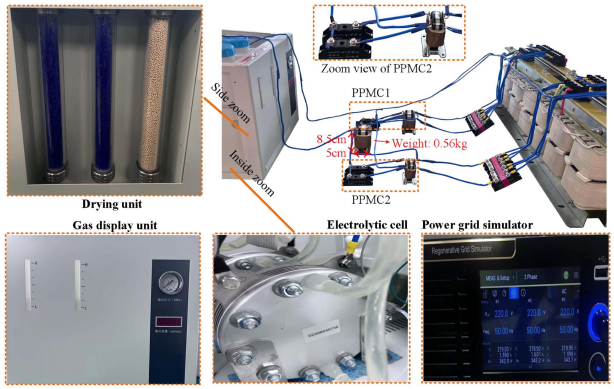

Fig. 7. Experimental setup.

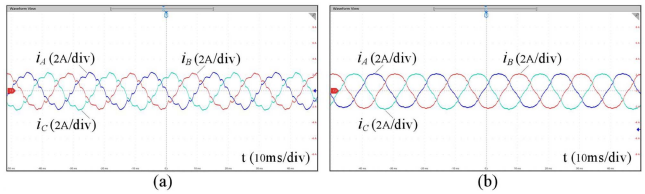

Fig. 8. Power quality analysis. (a) Experimental result of input current when not using PPMC. (b) Experimental result of input current when using PPMC.

B. Experimental Analysis

To further verify the feasibility of the proposed hydrogen production power supply, a 1-kW experimental prototype is implemented, as shown in Fig. 7. The resistor is connected in series with the EC to facilitate voltage division. Additionally, the input voltage of 380 Vac and the bus frequency of 50 Hz are maintained by the power grid simulator (Chroma 61815).

For power quality analysis, the experimental result is shown in Fig. 8(b). Taking into account the filtering characteristics of the leakage inductance from the phase-shifting transformer, the measured value of the input current's THD at 5.2% is marginally lower than the simulated value of 7.17%. As shown in Fig. 8(a), the THD observed in the rectifier without the PPMC is 13.7%, whereas the THD of the proposed rectifier has decreased by approximately 8.5%. Additionally, to accommodate the EC of different powers, Table II showcases a broader range of operating conditions. It reveals that the harmonic content of the grid-side current increases when the rectifier system operates under light-load conditions. However, whether under light load or full load, the proposed solution ensures that the grid-side current maintains low harmonic pollution levels and high power factor.

For the analysis of hydrogen production efficiency, the injection currents are analyzed and presented in Fig. 9. As shown in the simulation and experimental results in Fig. 9(a) and (b),

TABLE II
POWER QUALITY PARAMETERS UNDER DIFFERENT LOADS

Loads (%)	THD (%)	$i_{A\text{-}RMS}$ (A)	i_d (A)	PF (%)
20	7.0	0.342	5.287	99.1
40	6.1	0.682	10.571	99.3
60	5.6	1.023	15.853	99.4
80	5.4	1.363	21.133	99.5
100	5.2	1.703	26.411	99.5

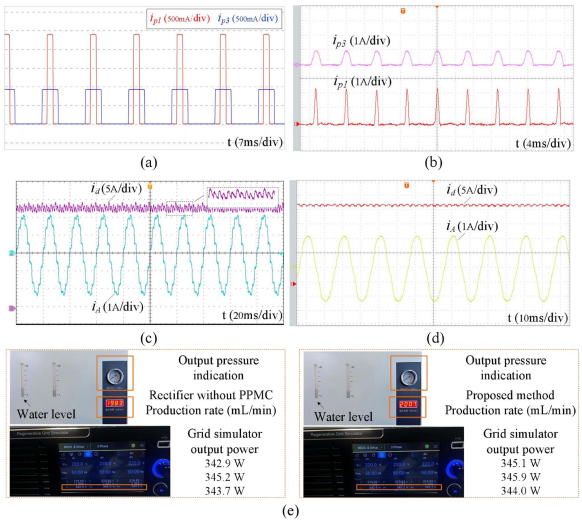

Fig. 9. Analysis of hydrogen production efficiency. (a) Simulation results of injection currents i_{p1} and i_{p3}. (b) Experimental results of injection currents i_{p1} and i_{p3}. (c) Experimental result of output current of rectifier without PPMC. (d) Experimental result of output current of the proposed method. (e) Display of H_2 meter of rectifier without PPMC and the proposed method.

the injection current forms a square wave with a frequency of 150 Hz. Due to the filtering effect of transformer leakage inductance, the measured currents i_{p1} and i_{p3} are smoother than the simulation results. Additionally, after the superposition of the currents i_{p1} and i_{p3}, more pulses appear, significantly suppressing current ripple. This comparison between the rectifier without PPMC and the proposed method is illustrated in Fig. 9(c) and (d). As a result, the ripple of the output current is reduced from 5.3% to 2.5%, indicating a significant reduction in the proportion of additional losses caused by current ripple in the EC with the proposed scheme. It is worth noting that the hydrogen production has increased from 1983 to 2007 mL/min, accompanied by a 1.2% increase in efficiency, as shown in Fig. 9(e). In addition, the hydrogen production rate of the EC is 1021 mL/min when it operates at half load with resistors connected in series. This is consistent with theoretical analysis, as there is an approximately proportional relationship between the hydrogen production and the current.

VI. CONCLUSION

In a quest to optimize multipulse rectifiers for hydrogen production, this article introduces a parallel 24-pulse rectifier employing DNPST. Comprehensive analysis is conducted on the operational specifications, input and output currents, as well as the capacity of magnetic devices. Through simulation and experimentation, the results reveal a mere 5.2% of input current harmonics and a minimal 2.5% output current ripple, showcasing the viability and effectiveness of the proposed technique. Furthermore, the proposed method offers the following advantages.

1) High efficiency, as the current flowing through the auxiliary unit accounts for a mere 3.4% of the output current.
2) DNPST serves to diminish manufacturing errors and facilitates favorable circumstances for large-scale production.
3) The parallel configuration presents robust fault tolerance and minimizes losses within the injection circuit.
4) Cost-effectiveness is ensured, along with the potential for power expansion, given that the power capacity of the auxiliary units represents only 6.6% and 4.3%, respectively.

REFERENCES

[1] J. Xiong, Y. Xia, Y. Peng, and W. Wei, "A multimode self-optimization electrolysis converting strategy for improving efficiency of alkaline water electrolyzers," *IEEE Trans. Power Electron.*, vol. 39, no. 3, pp. 3738–3748, Mar. 2024, doi: 10.1109/TPEL.2023.3346897.

[2] H. Tian, M. Chen, G. Liang, and X. Xiao, "A single-phase transformerless common-ground type PV inverter with active power decoupling," *IEEE Trans. Ind. Electron.*, vol. 70, no. 4, pp. 3762–3772, Apr. 2023, doi: 10.1109/TIE.2022.3181361.

[3] T. Song, Y. Zhang, F. Gao, X. Zhu, J. Shan, and Z. Kong, "Power model free voltage ripple suppression method of three-phase PWM rectifier under unbalanced grid," *IEEE Trans. Power Electron.*, vol. 37, no. 11, pp. 13799–13807, Nov. 2022, doi: 10.1109/TPEL.2022.3184403.

[4] G. Li, J. Ruan, K. Wang, Y. Deng, X. He, and Y. Wang, "An interleaved three-phase PWM single-stage resonant rectifier with high-frequency isolation," *IEEE Trans. Ind. Electron.*, vol. 67, no. 8, pp. 6572–6582, Aug. 2020, doi: 10.1109/TIE.2019.2938461.

[5] J. J. Sandoval, H. S. Krishnamoorthy, P. N. Enjeti, and S. Choi, "Reduced active switch front-end multipulse rectifier with medium-frequency transformer isolation," *IEEE Trans. Power Electron.*, vol. 32, no. 10, pp. 7458–7468, Oct. 2017, doi: 10.1109/TPEL.2016.2632717.

[6] R. Abdollahi, G. B. Gharehpetian, and M. Davari, "A novel more electric aircraft power system rectifier based on low-rating autotransformer," *IEEE Trans. Transp. Electrific.*, vol. 8, no. 1, pp. 649–659, Mar. 2022, doi: 10.1109/TTE.2021.3104576.

[7] S. P. P, R. Kalpana, K. S. Chethana, and B. Singh, "A 36-pulse AC–DC converter with DC-side tapped interphase bridge rectifier for power quality improvement," *IEEE Trans. Ind. Appl.*, vol. 57, no. 1, pp. 549–558, Jan./Feb. 2021, doi: 10.1109/TIA.2020.3028341.

[8] J. Wang, C. Zhao, T. Yu, T. Liu, X. Yao, and Q. Chen, "New 24-pulse rectifier with passive current injection circuit based on dual auxiliary transformers," *IEEE J. Emerg. Sel. Topics Power Electron.*, vol. 11, no. 5, pp. 5321–5336, Oct. 2023, doi: 10.1109/JESTPE.2023.3308188.

[9] J. Wang, T. Yu, C. Zhao, T. Liu, X. Yao, and Q. Chen, "A simple 24-pulse star rectifier combining two different tap converters," *IEEE Trans. Transp. Electrific.*, vol. 9, no. 3, pp. 3978–3993, Sep. 2023, doi: 10.1109/TTE.2023.3244790.

[10] J. Wang, T. Liu, T. Yu, C. Zhao, X. Yao, and Q. Chen, "A series-connected 24-pulse star rectifier employing two different pulse-doubling interphase reactors," *IEEE Trans. Power Electron.*, vol. 39, no. 1, pp. 1460–1481, Jan. 2024, doi: 10.1109/TPEL.2023.3323795.

[11] F. J. Chivite-Zabalza, A. J. Forsyth, and D. R. Trainer, "A simple, passive 24-pulse AC–DC converter with inherent load balancing," *IEEE Trans. Power Electron.*, vol. 21, no. 2, pp. 430–439, Mar. 2006, doi: 10.1109/TPEL.2005.869754.

[12] S. Yang, J. Wang, and W. Yang, "A novel 24-pulse diode rectifier with an auxiliary single-phase full-wave rectifier at DC side," *IEEE Trans. Power Electron.*, vol. 32, no. 3, pp. 1885–1893, Mar. 2017, doi: 10.1109/TPEL.2016.2560200.

[13] F. Meng, Q. Du, L. Wang, L. Gao, and Z. Man, "A series-connected 24-pulse rectifier using passive voltage harmonic injection method at DC-link," *IEEE Trans. Power Electron.*, vol. 34, no. 9, pp. 8503–8512, Sep. 2019, doi: 10.1109/TPEL.2018.2889507.